2008

Participation of Aluminum Hydride in the Anodic Dissolution of Aluminum in Alkaline Solutions

Saikat Adhikari
Iowa State University

Kurt R. Hebert
Iowa State University, krhebert@iastate.edu

Journal of The Electrochemical Society, **155** (5) C189-C195 (2008)
0013-4651/2008/155(5)/C189/7/$23.00 © The Electrochemical Society

Participation of Aluminum Hydride in the Anodic Dissolution of Aluminum in Alkaline Solutions

Saikat Adhikari* **and Kurt R. Hebert****,z**

Department of Chemical and Biological Engineering, Iowa State University, Ames, Iowa 50011, USA

The mechanism of anodic alkaline dissolution of aluminum was investigated through the analysis of cyclic voltammetry (CV) and potential step experiments. Attention was focused on the role of aluminum hydride (AlH_3) as a reaction intermediate, as suggested by the recent detection of AlH_3 formation during open-circuit dissolution. Potential step experiments at pH 11.75 revealed that the potential at the metal–surface film interface was close to the Nernst potential of AlH_3 oxidation. This finding suggested a reaction mechanism in which an interfacial AlH_3 layer is formed continuously by reaction of cathodically formed H with Al, and is then oxidized to the dissolution product, aluminate $[Al(OH)_4^-]$ ions. However, potential step experiments at pH 11 did not indicate the presence of interfacial AlH_3; instead, the metal–film interface was close to the equilibrium potential of Al oxidation. Analysis of the CV indicated an abrupt transition in dissolution behavior between the two pH values, from a relatively rapid dissolution controlled by diffusion and film conduction in highly alkaline solutions, to a slow dissolution at a lower pH controlled by a highly resistive surface film. The formation of interfacial AlH_3 occurs readily at the higher pH, but is suppressed as the pH approaches neutrality.
 [DOI: 10.1149/1.2883827]

Manuscript submitted November 20, 2007; revised manuscript received January 17, 2008.
Available electronically March 11, 2008.

The electrochemical dissolution of aluminum and its alloys in alkaline solutions is technologically relevant as the anode reaction in aluminum–air batteries.[1] This interest in batteries has led to a number of mechanistic studies of the dissolution process. In moderately basic solutions, the rate of anodic dissolution may be controlled by the combination of electrode kinetics, mass transport, or conduction through a surface film.[2-7] The dissolution reaction mechanism in concentrated KOH solutions was investigated by Macdonald et al. using electrochemical impedance spectroscopy.[8] They determined that the metal corrodes by a reaction pathway in which OH^- ions are added sequentially to Al atoms, until the stable aluminate ion, $Al(OH)_4^-$, is formed. A different view of the mechanism is suggested by a study by Perrault, which indicated that the oxidation of aluminum hydride, AlH_3, may by involved in the dissolution.[9] He showed that the open-circuit potential of Al in alkaline solutions corresponds closely to the Nernst potential for hydride oxidation. In support of the possible role of hydride, Despić and co-workers observed that polarization at cathodic potentials generates a product with an oxidation potential close to that of aluminum hydride.[10,11]

In a recent secondary ion mass spectrometry investigation, we showed that submicrometer AlH_3 particles are formed as a product of open-circuit Al dissolution in 1 M NaOH solution at room temperature.[12] Potential measurements indicated that the dissolution potential was close to the Nernst potential for oxidation of the hydride. It was proposed that AlH_3 is continuously created through the etching of Al by cathodically generated hydrogen atoms

$$H_2O + e^- \rightarrow OH^- + H \quad [1]$$

$$Al + 3H \rightarrow AlH_3 \quad [2]$$

Evidence for Reaction 2 has been found in a number of vacuum studies of H interactions with clean Al surfaces.[13-18] The hydride then oxidized according to the reaction identified by Perrault

$$AlH_3 + 7\ OH^-(aq) \rightarrow Al(OH)_4^- + 3H_2O(aq) + 6e^- \quad [3]$$

In this mechanism Reaction 3 is close to equilibrium, and so its Nernst potential determines the open-circuit potential during dissolution. The overall open-circuit reaction formulated by the combination of these reactions accounts for the observed formation of AlH_3

$$2Al + OH^- + 3H_2O \rightarrow Al(OH)_4^- + AlH_3 \quad [4]$$

The present paper examines whether the electrochemical behavior of anodic Al dissolution in alkaline solutions supports the participation of AlH_3 as a reaction intermediate. Results of cyclic voltammetry (CV) and potential step experiments are interpreted using models for the Al electrode based on the proposed mechanism. In particular, because AlH_3 formation by Eq. 2 should occur at the Al surface, the hydride is assumed to be present as a layer of unknown thickness in contact with the metal. The hydride may also be covered by a precipitated $Al(OH)_3$ overlayer, in view of some evidence for such a layer during alkaline dissolution.[2-5] Indeed, there is a substantial driving force for $Al(OH)_3$ formation, because the open-circuit potential is about 0.5 V positive to the Nernst potential of Al oxidation.[19] The present experiments sought to identify the potential at the interface of the metal and this surface film, and to determine whether it corresponds to the Nernst potential for the oxidation of aluminum hydride.

Experimental

CV and potential step experiments were carried out in 0.1 M Na_2SO_4 solutions adjusted to the pH of either 11 or 11.75. These pH values were selected for the following reasons. First, they lie within the pH range in which the open-circuit potential is close to the Nernst potential of hydride oxidation (Eq. 3), suggesting the possible presence of interfacial hydride.[9] Second, at these pH values currents due to cathodic reactions are not significant above the open-circuit potential, thus facilitating interpretation of the current measurements in terms of anodic processes. Finally, this pH range embodies the transition between the rapid dissolution of Al found in alkaline solutions and its passive behavior in neutral solutions.[19] Thus, the results allow us to suggest whether the AlH_3 mechanism might be relevant to either or both of these regimes of the Al electrode.[7]

The Al samples were 110 μm thick foils of 99.99% purity (Toyo). The foil was provided in the as-annealed condition, and its grain size was roughly 100 μm. No evidence for grain boundary attack was found during a microscopic examination of the samples after alkaline treatments.[12] Solutions for all experiments were prepared using reagent grade chemicals and Nanopure water. Prior to voltammetry, the samples were treated by electropolishing and caustic etching. Electropolishing was carried out in a solution of 20% $HClO_4$ in ethanol at 5°C and 30 V for 5 min. The samples were then washed in deionized water and mounted in a glass electrochemical cell used for both alkaline treatment and voltammetry. The exposed sample area in the cell was 1.77 cm^2. The edge of the electropol-

* Electrochemical Society Student Member.
** Electrochemical Society Active Member.
z E-mail: krhebert@iastate.edu

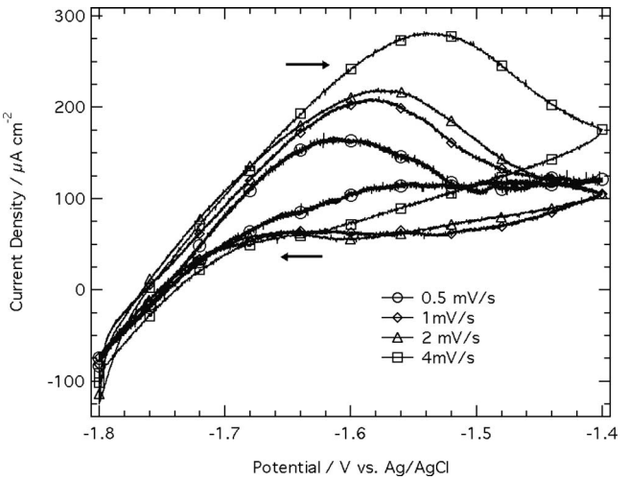

Figure 1. CV response at pH 11.75.

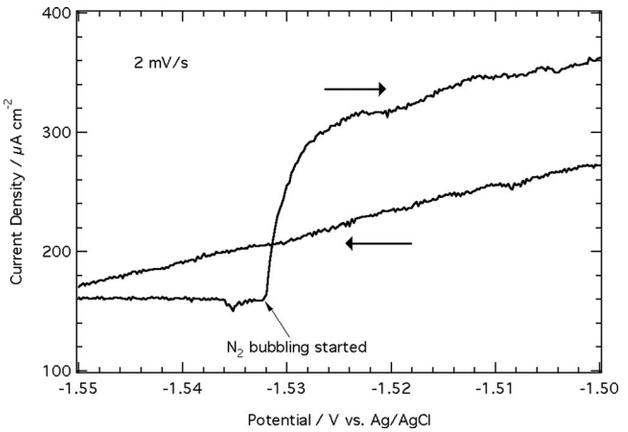

Figure 2. Effect of stirring on current measured during voltammetric scan.

ished area was deliberately covered because of indications that preferential dissolution had occurred in this region. Alkaline etching was at open circuit in 1 M NaOH solution for a period of 1 min at 21°C.

After alkaline treatment, the cell solution was replaced with 0.1 M Na_2SO_4, with its pH adjusted to either 11 or 11.75 by the addition of NaOH crystals. A potentiostat was used to apply electrochemical polarization, using a Pt wire counter electrode and a Ag/AgCl reference electrode. The cited potentials are expressed relative to Ag/AgCl unless otherwise specified. Because the currents measured during CV were found to be temperature-sensitive, the temperature was controlled at 21°C. The solutions were typically air-saturated, but in some experiments deaeration was accomplished by nitrogen sparging for 60 min. Two types of electrochemical experiments were carried out, CV and potential step experiments. CV experiments were initiated by scanning in the anodic direction from a potential near open circuit. In the potential step experiments, the Al electrode was first held at a constant potential above open circuit for 5 min, in order to obtain a steady-state passive current density. Then, a sequence of positive 0.1 V potential steps at 10 ms intervals was executed, and the resulting current transients recorded. As described in detail below, current–potential plots were obtained from these data which revealed characteristics of conduction in the surface film, and indicated the potential at the metal–film interface.

The cell ohmic resistance, which was required for analysis of both CV and potential step experiments, was obtained by anodically etching aluminum foils in 1 M HCl solution, in the same cell.[20] The etching current density was shown to be controlled by the cell ohmic resistance. The cell resistance during etching was multiplied by the ratio of the conductivity of 0.1 M Na_2SO_4 to that of 1 M HCl, to obtain the cell resistance applicable to the present experiments. The resistance was found to be 300 Ω cm^2.

Results and Discussion

CV.— Figure 1 shows four CV experiments at scan rates between 0.5 and 4 mV/s, in air-saturated pH 11.75 solution. Deaeration by nitrogen sparging was found to suppress cathodic currents, but had no significant effect on currents in the anodic potential region, the main focus of attention. Each positive scan in Fig. 1 displayed a broad current density maximum between 150 and 300 $\mu A/cm^2$, which increased with scan rate. Both the peak shape and the effect of the scan rate are qualitatively consistent with at least partial diffusion control of the anodic reaction rate.[21] The influence of diffusion was explicitly demonstrated in an experiment in which the bubble stream from a nitrogen sparger was positioned near the Al surface (Fig. 2). The sudden initiation of stirring by bubbles caused the current nearly to double within a time of 4 s, clearly indicating a sensitivity to mass transport. The same conclusion was reached by Heusler and Allgaier in their rotating-disk electrode study of Al dissolution at comparable pH values.[7] However, the anodic peak currents in Fig. 1 increase more slowly with scan rate than the one-half power dependence expected for pure diffusion control, and the peak potentials shift in the positive direction at higher scan rates. This behavior may be attributed to the additional influence of electrode kinetics and/or surface film conduction.[21] Therefore, quantitative characterization of conduction and kinetics, with the help of the potential step experiments, was necessary for the interfacial potential to be determined.

CV results in pH 11 Na_2SO_4 solution are shown in Fig. 3. Upon initiation of the scans, the anodic current density increased rapidly to peaks at about 90 $\mu A/cm^2$, and subsequently decayed to much lower current densities of 20–30 $\mu A/cm^2$. The current density in the second positive scan (dashed lines) remained below 20 $\mu A/cm^2$. Aside from the initial anodic peaks, the anodic currents at pH 11 were much lower than those at pH 11.75. The high sensitivity to pH is not surprising, as the open-circuit corrosion rate decreases by an order of magnitude as the pH is reduced from 12 to 11.[19] In contrast to the results at pH 11.75 (Fig. 1), the peak currents in Fig. 3 did not depend on the scan rate. Indeed, as Fig. 4 demonstrates, the anodic current peaks and decays depended only on the elapsed time during the scan, and were independent of potential. Evidently, these transients resulted from time-dependent processes accompanying the start of the experiment, after the Al samples were

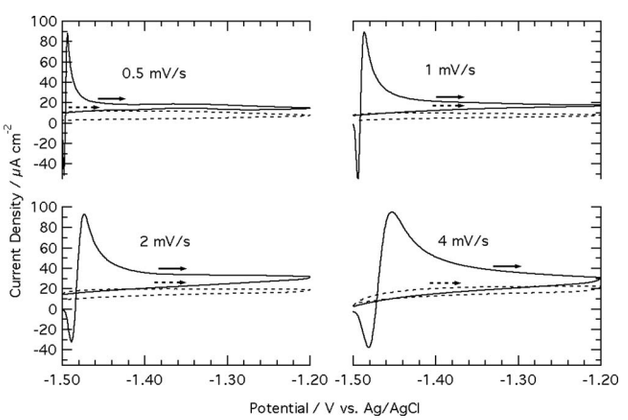

Figure 3. CV response at pH 11. The solid and dashed lines represent the first and second voltage cycles, respectively.

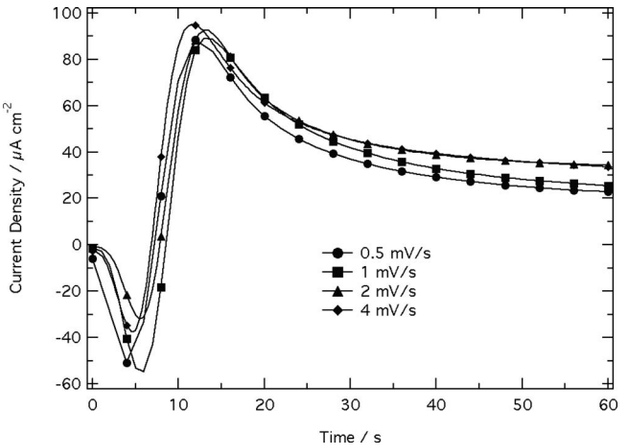

Figure 4. Current density measured during initial portion of first positive sweeps in Fig. 3, plotted against elapsed time during the potential scan.

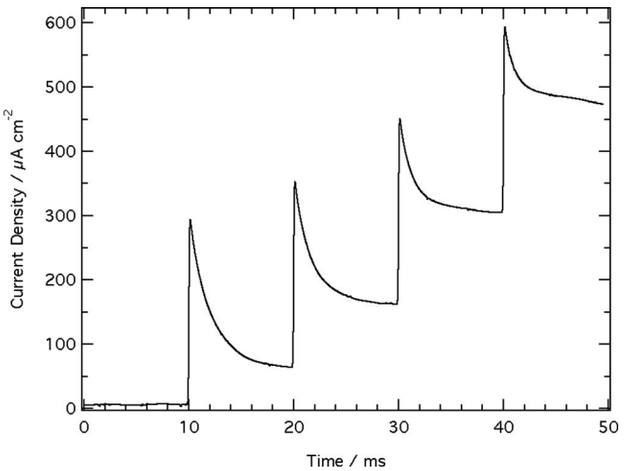

Figure 5. Example of current response to sequence of applied potential steps. The applied potential was initially held at −1.55 V for 5 min, during which a steady passive current was obtained. Then, the potential was stepped by 0.1 V in the positive direction, at 10 ms intervals.

transferred from the 1 M NaOH pretreatment bath (pH 13.5) to the pH 11 Na_2SO_4 solution. The modeling results presented below will help to clarify the nature of these processes.

After the initial decays, the currents in the first positive scan approached constant values. The positive scans during the second CV cycles exhibited no initial anodic peaks, and instead showed anodic plateaus below 20 $\mu A/cm^2$. A similar CV response was demonstrated previously in the neutral pH range by Isaacs, White, and their co-workers.[22-25] They showed that the anodic plateaus were due to currents controlled by ionic conduction through a highly resistive surface film exhibiting high-field conduction. Evidently, over the narrow pH range from 11.75 to 11, there is an abrupt transition from diffusion-sensitive dissolution rates, characteristic of alkaline solutions, to passive behavior dominated by a resistive surface film, as typically found in neutral solutions.

Potential step experiments.— Potential step experiments were carried out to determine the potential at the metal/film interface, through analysis of the potential drop through the surface film. The procedure of these experiments was first developed by Hurlen and Haug.[26] As described in the Experimental section, the Al electrode was first held at a constant potential above open circuit, in order to establish a steady-state passive current density. At steady state, the surface film thickness (δ_{ss}) was given by

$$E_{init} = E_{m/f} + \frac{\delta_{ss}}{B}\ln\left(\frac{i_{ss}}{i_{ao}}\right) \quad [5]$$

where E_{init} is the initial applied potential, $E_{m/f}$ is the potential at the metal/film interface, and the second term on the right represents the potential drop through a high-field conducting surface film, in which the current increases exponentially with electric field. In this term, i_{ss} is the approximately potential-independent steady-state passive current density; i_{ao} and B are the pre-exponential current density and field coefficient in the high-field conduction rate equation.

After the potential hold at E_{init}, a sequence of 0.1 V potential steps was applied at 10 ms intervals, resulting in a transient current response like the example shown in Fig. 5. Each voltage step was immediately followed by an exponential current decay. This transient decay is attributed to capacitive charging, because the decay time of about 10 ms is consistent with the capacitive time constant of 3 ms estimated from the cell resistance of 300 Ω cm^2 and a typical capacitance of 10 $\mu F/cm^2$ for Al.[27] After the capacitive transient, the current continued to decay more slowly, due primarily to anodic film growth. However, calculations based on Faraday's law indicated that no significant film growth would have occurred during the 40 ms time interval of the step sequence. Also, this time interval is too short for diffusion to produce significant changes in the solution composition near the Al surface. Therefore, the current at 10 ms after each step (i_{step}) represented the conduction current density passed through the initial steady-state film thickness δ_{ss}

$$i_{step} = i_{ao}\exp\left[\frac{B(E_{step} - E_{m/f})}{\delta_{ss}}\right] \quad [6]$$

where E_{step} is the applied potential during the step, after correction for cell ohmic resistance. Figures 6 and 7 show that, at both pH values, i_{step} varies exponentially with E_{step}, as expected from Eq. 6. Also, the figures indicate that the slope $d\ \ln\ i_{step}/dE_{step}$ decreases with increasing values of the initial potential E_{init}. This trend is attributable to the increasing steady-state film thickness with E_{init}, according to Eq. 5, and is evidence that the exponential current–potential relations in Fig. 6 and 7 are controlled by conduction rather than electrochemical kinetics.

According to Eq. 6, the inverse slopes in Fig. 6 and 7, $dE_{step}/d\ \ln\ i_{step}$, are directly related to the steady-state film thickness δ_{ss}. From Eq. 5, the inverse slope is expected to depend linearly on the initial applied potential

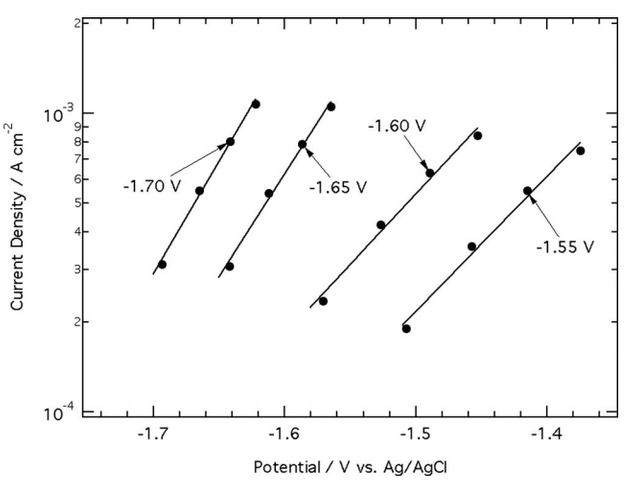

Figure 6. Examples of current–potential characteristics, obtained from the sequential potential step experiments at pH 11.75. Results are shown for various applied steady-state potentials prior to the potential steps.

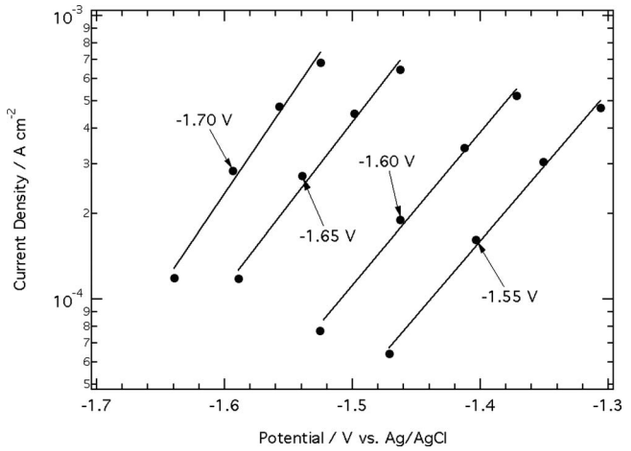

Figure 7. Examples of current–potential characteristics, obtained from sequential potential step experiments at pH 11. Results are shown for various applied steady-state potentials prior to the potential steps.

$$\frac{dE_{\text{step}}}{d\ \ln\ i_{\text{step}}} = \frac{E_{\text{init}} - E_{\text{m/f}}}{\ln\dfrac{i_{\text{ss}}}{i_{\text{ao}}}} \qquad [7]$$

In Fig. 8, the inverse slopes from all the potential step experiments at pH 11 and 11.75 are plotted against the initial applied potential. The data were well approximated by different linear potential dependences at the two pH values. Equation 7 indicates that the extrapolations of the regression lines to the potential axis should provide estimates of the interfacial potential $E_{\text{m/f}}$. At pH 11, $E_{\text{m/f}}$ was found to be −2.34 V, nearly identical to the Nernst potential for the oxidation of Al to $Al(OH)_3$ or Al_2O_3, −2.32 V.[19] We conclude that the film composition at the interface is close to aluminum hydroxide or oxide. $E_{\text{m/f}}$ at pH 11.75 was −1.92 V vs Ag/AgCl, a value close to the Nernst potential of AlH_3 oxidation, −1.82 V.[9] For hydride oxidation to determine the interfacial potential, a high fraction of the metal/film interface should be in direct contact with AlH_3 as opposed to aluminum oxide or hydroxide. This result supports the proposed reaction scheme involving AlH_3 as an intermediate: evidently, aluminum hydride is formed continuously by the reaction of Al with cathodically generated H (Eq. 1 and 2), even under anodic

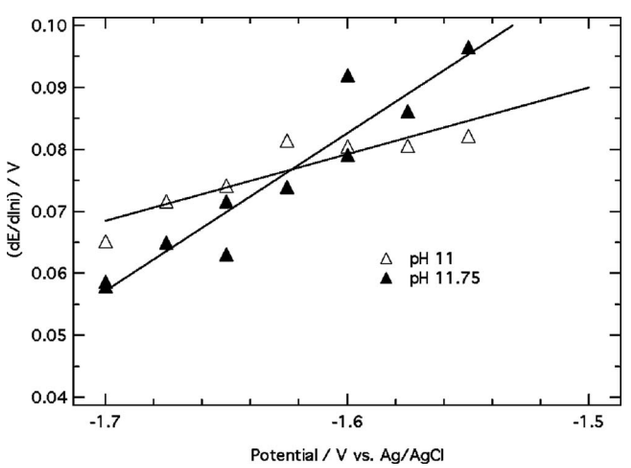

Figure 8. Reciprocal slopes of current–potential characteristics at pH 11 and 11.75, plotted against the applied steady-state potential prior to potential steps. Lines are linear regressions of the data. The zero-current intercepts of the regression lines are −2.32 V (pH 11) and −1.92 V (pH 11.75).

polarization. It is concluded that the interface composition during anodic polarization differs qualitatively between these two closely separated pH values. The results do not preclude the possibility that the entire film may be composed of AlH_3. In the next section, these interface compositions are used as a basis for modeling the CV experiments.

Mathematical Models

According to the discussion of the CV experiments, different processes control the dissolution rate at the two tested pH values. The current at pH 11.75 is influenced by solution phase diffusion and film conduction, while the film conduction resistance dominates at pH 11. Different models were formulated to simulate the CV at the two pH values. Both models considered only anodic electrochemical reactions, and were not intended to apply below the open-circuit potential.

Model for dissolution at pH 11.75.— In this model, we assume that the potential at the metal–film interface is close to the Nernst potential of the anodic hydride oxidation reaction (Eq. 3). The potential is given by

$$E = E^o_{AlH_3} - 2.303\frac{RT}{F}\text{pH}_\text{b} + \frac{RT}{6F}\ln\frac{y_{\text{As}}}{y^7_{\text{OHs}}} + \phi + iR_\text{s} \qquad [8]$$

where E is the measured potential relative to the standard hydrogen electrode (NHE), and the standard potential $E^o_{AlH_3}$ represents

$$E^o_{AlH_3} = \frac{1}{6F}\left|\mu^o_{Al(OH)_3} + 3\mu^o_{H_2} - 3\mu^o_{H_2O} - \mu^o_{AlH_3}\right| \qquad [9]$$

Using the AlH_3 standard chemical potential of 25 kcal/mol cited by Perrault, E^o_A is found to be −0.957 V vs NHE. The second term on the right of Eq. 8 corrects for the bulk pH (pH_b), the third term is the concentration overpotential, and the remaining terms are the potential drops through the surface film (ϕ) and across the cell ohmic resistance (iR_s). In the concentration overpotential, y_{OHs} and y_{As} are dimensionless concentrations of hydroxide and aluminate ions close to the electrode surface. y_{OHs} is defined according to $y_{\text{OHs}} = [OH^-]_\text{s}/[OH^-]_\text{b}$, where $[OH]_\text{s}$ and $[OH^-]_\text{b}$ are the surface and bulk OH^- concentrations. y_{As} is $[Al(OH)^-_4]\text{s}/[Al(OH)^-_4]^{\text{sat}}_\text{b}$, where $[Al(OH)^-_4]\text{s}$ is the surface concentration of aluminate ions and $[Al(OH)^-_4]^{\text{sat}}_\text{b}$ represents the concentration of aluminate ions in equilibrium with solid $Al(OH)_3$ at the bulk solution pH. $[Al(OH)^-_4]^{\text{sat}}_\text{b}$ depends on the bulk pH according to $[Al(OH)^-_4]^{\text{sat}}_\text{b} = K_4[OH^-]_\text{b}$, where K_4 is the equilibrium constant of $Al(OH)_3$ formation. The potential drop in the film was obtained from the results of potential step experiments at the initial potential of −1.7 V

$$\phi = \frac{1}{b}\ln\left(\frac{i}{i_{\text{ao}}}\right) \qquad [10]$$

where the parameters b and i_{ao} were taken from the slope and intercept of the regression fit in Fig. 6 at −1.7 V.

The near-surface concentrations of OH^- or $Al(OH)^-_4$ ions in Eq. 8 were obtained by solving the diffusion equations for these species

$$\frac{\partial\, y_i}{\partial\, t} = D_i\frac{\partial^2 y_i}{\partial\, z^2} \qquad [11]$$

where i can be OH^- or $Al(OH)^-_4$. The concentration of Na_2SO_4 supporting electrolyte was considered to be high enough so that the migration flux in the diffusion layer could be neglected relative to the diffusion flux. The boundary conditions at the electrode surface are

$$\left.\frac{\partial\, y_{\text{OH}}}{\partial\, z}\right|_{z=0} = \frac{4i}{3\text{FD}_{\text{OH}}[OH^-]_\text{b}} \qquad [12]$$

$$\left.\frac{\partial y_{Al}}{\partial z}\right|_{z=0} = -\frac{D_{OH}}{4D_{Al}K_4}\left.\frac{\partial y_{OH}}{\partial z}\right|_{z=0} \quad [13]$$

The boundary conditions in the bulk solution, i.e., as z approaches infinity, are $y_{OH} = 1$ and $y_{Al} = 0$. Equations 11-13 were solved numerically. The diffusivities D_{OH} and D_{Al} were 5.3×10^{-5} and 8.4×10^{-6} cm^2/s, respectively.[7,28] The equilibrium constant K_4 was 0.05.[29] The values of all model parameters were known from the potential step experiments or other sources.

Model for dissolution at pH 11.— According to the results of the potential step experiments, this model assumes that the reaction at the metal/film interface is the direct oxidation of Al. The potential at this interface is the Nernst potential of the Al oxidation reaction, and the current is controlled by high-field conduction in the surface film. The concentration overpotential and ohmic drop are neglected because the large conduction resistance leads to low current densities of tens of μA/cm^2. With these assumptions, the electrode potential may be related to the Nernst potential for the oxidation of Al

$$E = E^o_{Al} - 2.303\frac{RT}{F}pH_b + \phi \quad [14]$$

where the standard potential E^o_{Al} is

$$E^o_{Al} = \frac{1}{3F}\left[\frac{3}{2}\mu^o_{H_2} - 3\mu^o_{H_2O} - \mu^o_{Al} + \mu^o_{Al_2O_3}\right] \quad [15]$$

which has the value −1.50 V vs NHE.[19] The model assumes that the film composition is Al_2O_3 because the conduction parameters of the oxide are known from studies of anodic films.[30]

The current through the film/solution interface is carried by ion-transfer processes, whereby OH^- or H_2O in solution react to form O^{-2} ions in the film, and Al^{+3} ions in the film are ejected to form $Al(OH)_4^-$ ions in solution.[31] It is necessary to characterize these processes, because O^{-2} transfer leads to film growth or dissolution, which affects the conduction resistance. In view of the very low current densities in Fig. 3, along with the typically facile kinetics of oxygen transfer,[31] the potential drop at the film/solution interface is assumed to be close to equilibrium with respect to the O^{-2} transfer process. Further, since the kinetics of metal ion transfer is relatively sluggish, this constant interfacial potential drop implies that the metal ion transfer current density is approximately fixed at a value i_{co}. The rate of film growth or dissolution during the CV experiment can then be written as

$$\frac{d\delta}{dt} = \frac{(i - i_{co})\Omega_{ox}}{6F} \quad [16]$$

where δ is the film thickness and Ω_{ox} is the molar volume of the oxide. The quantity $i - i_{co}$ represents the portion of the current density passing the film/solution interface which leads to the formation of O^{-2} ions in the film. The conduction current density i is related to the electric field in the film by the high-field conduction law, $i = i_{ao}\exp(B\phi/\delta)$. A differential equation for $i(t)$ was obtained by substituting for $d\delta/dt$ into Eq. 16 from the high-field conduction equation. The result is

$$\frac{di}{dt} = \frac{iv}{\phi}\frac{\ln(i/i_{ao})}{\left[1 - \ln(i/i_{ao})\frac{\Omega_{ox}(i - i_{co})}{6FBv}\right]} \quad [17]$$

where v is the voltage scan rate dE/dt during CV. The parameters i_{ao}, B, and Ω_{ox} were assigned values characteristic of anodic oxide films: 2.0×10^{-15} A/cm^2, 3.44×10^{-6} cm/V, and 32.9 cm^3/mol, respectively.[30]

The present CV model is mathematically the same as previous models for the CV of aluminum in neutral pH.[22-25] Both prior models incorporate high-field conduction, as is done here, along with an expression for the "oxide dissolution rate" which is related to the present metal ion dissolution current density i_{co}. For example, i_{co} is equivalent to R_{dis}/nF in Ref. 22, in which R_{dis} is the oxide dissolution rate. While the resulting models are equivalent, the present formulation is fundamentally more valid, because it incorporates the view that metal and oxygen ions in the film transfer individually to and from the aqueous solution. Requiring Al_2O_3 to dissolve as a stoichiometric entity, as in the prior models, implies that no current is passed at the film/solution interface, and therefore violates the continuity of the interface and conduction current.

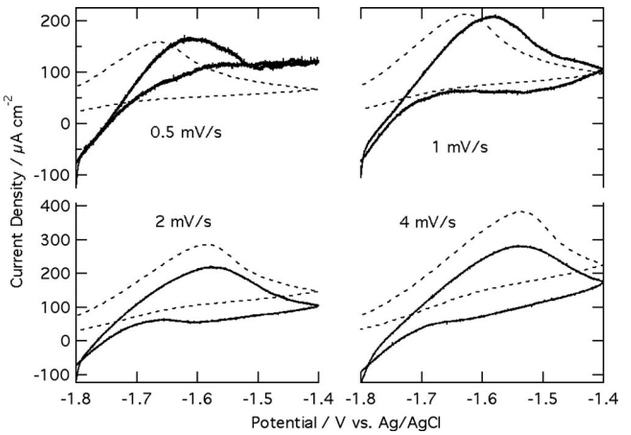

Figure 9. Comparison of experimental (solid lines) and simulated (dashed lines) CV responses at pH 11.75, at various scan rates.

When Eq. 17 was integrated with i_{co} taken to be constant, the predicted CV results displayed anodic current plateaus similar to those in the earlier models, but the anodic current peaks in the first scan of experimental CVs (Fig. 3 and 4) were absent. Anodic peaks in the simulated CV could be obtained when a transient decay of i_{co} was introduced

$$i_{co} = i^f_{co} + (i^i_{co} - i^f_{co})\exp\left(-\frac{t}{t_c}\right) \quad [18]$$

Here, i^i_{co} and i^f_{co} are the initial and final values of i_{co}, and t_c is the time constant associated with its decay. The time dependence of i_{co} may derive from the sensitivity of the kinetics of metal ion transfer to the chemical composition of the oxide surface, which in turn depends on the solution pH. The decay in Eq. 18 would be caused by the relaxation of the oxide surface from its initial state in the 1 M NaOH pretreatment solution, to its final condition in the pH 11 solution used in CV experiments. The pH-dependent surface composition may reflect a change of the overall film composition from AlH_3 in 1 M NaOH to aluminum oxide or hydroxide at pH 11.

Comparison of experimental results with model calculations.— In Fig. 9, predictions of the CV model based on AlH_3 oxidation at the metal/film interface (Eq. 8-13) are compared with the experimental results at pH 11.75. Particularly in view of the absence of adjustable fitting parameters, the figure demonstrates an excellent agreement between the shapes of predicted and experimental CV waveforms. The deviation near the open-circuit potential was expected, because cathodic reactions were not included in the model. The discrepancy of anodic peak currents and potentials at higher scan rates may also relate to simplifications inherent in the model. In particular, Fig. 6 indicates that the surface film thickness depends on potential, while the model assumes a constant conduction resistance. Film growth and dissolution were not included because the film/solution interface kinetics is unknown. Nonetheless, the overall very good agreement exhibited in Fig. 8 is additional evidence that the interfacial potential is controlled by the AlH_3 oxidation reaction.

The calculations from the Al oxidation model (Eq. 17 and 18) are compared to experimental CV in Fig. 10 and 11. Figure 10 shows the first CV cycle and Fig. 11 the second. In order to fit the model to the experiment, the initial film thickness was set to 1.7 nm, and i^i_{co},

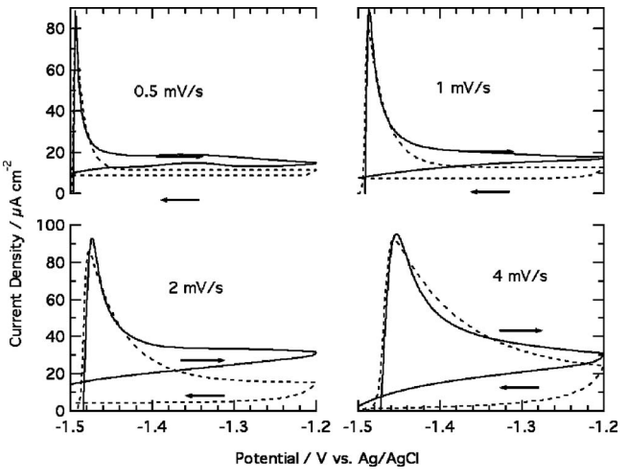

Figure 10. Comparison of experimental (solid lines) and simulated (dashed lines) CV responses at pH 11. First scan for various scan rates.

i_{co}^{f}, and t_c were 135 μA/cm^2, 10 μA/cm^2, and 20 s, respectively. When these parameters were applied to all scan rates, the model calculations agreed very well with experimental CV. The model captured the effects of scan rate on the time of the anodic peak, and the subsequent current decay during the first positive scan. Again, this agreement supports the view that these features are caused by a time-dependent i_{co} (Eq. 18), associated with an adjustment of the film surface to the reduction of pH from 13.5 to 11. By the outset of the second CV cycle, i_{co} had reached its final constant value, i_{co}^{f}. During the second cycle, the model predicts anodic current plateaus similar to those found at neutral pH, the heights of which increase with scan rate as in the experimental CV. The overall excellent agreement with experimental CV supports the concept that high-field conduction in the surface film controls the anodic current.

In the alkaline pH range in which AlH_3 mediates dissolution, corrosion is accompanied by the formation of large subsurface metallic voids, and rapid absorption of H into the metal.[32,33] The hydride layer in direct contact with the metal could facilitate the formation of associated hydrogen-vacancy defects during dissolution.[33] These defects in turn could be responsible for the observed high rates of void formation and hydrogen injections. These processes are of potential importance for the fundamental understanding of surface chemical processes leading to hydrogen embrittlement and stress corrosion cracking.

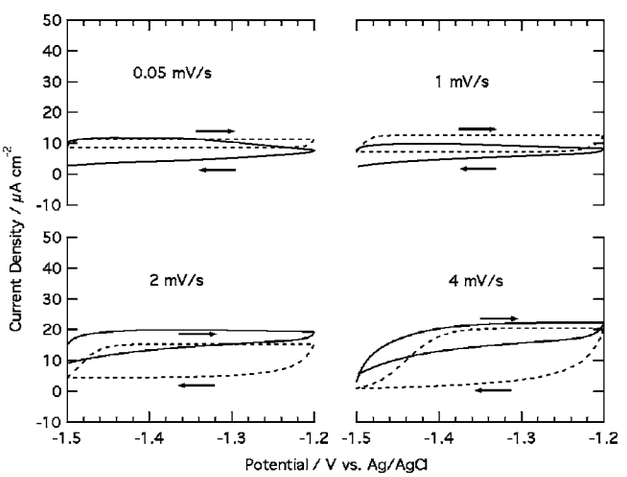

Figure 11. Comparison of experimental (solid lines) and simulated (dashed lines) CV responses at pH 11. Second scan for various scan rates.

Conclusions

The mechanism of Al dissolution in alkaline solutions was investigated by analysis of CV and potential step experiments. An abrupt transition of the surface film properties and dissolution mechanism was demonstrated in the pH range from 11 to 11.75. At pH 11, the behavior of the Al electrode is similar to that in neutral pH solutions, controlled by the anodic formation of a surface film with a high ionic conduction resistance. The potential at the metal/film interface indicates that the primary anodic reaction is Al oxidation. At pH 11.75, the surface film resistance is significantly reduced, and the consequently much larger dissolution current is strongly influenced by mass transport and ohmic resistance. Anodic metal dissolution is mediated by the formation and oxidation of interfacial aluminum hydride. The presence of interfacial AlH_3 during anodic polarization at pH 11.75 suggests that water transport to the metal/film interface is fast enough so that hydride can form before Al^{+3} ions can be transported away from the interface. The film structure and possibly composition is apparently quite different between the two pH values: the film at pH 11.75 seems to possess an appreciably lower conduction resistance and higher water permeability than the film at pH 11. These structural differences may correlate with the high sensitivity of oxide solubility to pH in this range.[19] In view of the present results, it is possible that the film at pH 11.75 and higher consists primarily of aluminum hydride. The interfacial hydride layer may assist the high rates of hydrogen absorption and open-volume defect formation in the metal, as observed in alkaline solutions.

Acknowledgments

Financial support was provided by St. Jude Medical Corp. and by the National Science Foundation through grant no. NSF-DMR-0605957.

Iowa State University assisted in meeting the publication costs of this article.

References

1. Q. F. Li and N. J. Bjerrum, *J. Power Sources*, **110**, 1 (2002).
2. R. Greef and C. F. W. Norman, *J. Electrochem. Soc.*, **132**, 2362 (1985).
3. O. R. Brown and J. S. Whitley, *Electrochim. Acta*, **32**, 545 (1987).
4. D. Chu and R. F. Savinell, *Electrochim. Acta*, **36**, 1631 (1991).
5. M. L. Doche, J. J. Rameau, R. Durand, and F. Novel-Cattin, *Corros. Sci.*, **41**, 805 (1999).
6. H. Kaesche, *Z. Phys. Chem.*, **34**, 87 (1962).
7. K. E. Heusler and W. Allgaier, *Werkst. Korros.*, **22**, 297 (1971).
8. D. D. Macdonald, S. Real, S. I. Smedley, and M. Urquidi-Macdonald, *J. Electrochem. Soc.*, **135**, 2410 (1988).
9. G. G. Perrault, *J. Electrochem. Soc.*, **126**, 199 (1979).
10. A. R. Despić, D. M. Drazic, J. Balaksina, L. Gajickrstajic, and R. M. Stevanovic, *Electrochim. Acta*, **35**, 1747 (1990).
11. J. Radosevic, M. Kliskic, P. Dabic, R. Stevanovic, and A. Despic, *J. Electroanal. Chem.*, **277**, 105 (1990).
12. S. Adhikari, J. Lee, and K. R. Hebert, *J. Electrochem. Soc.*, **155**, C16 (2008).
13. M. Hara, K. Domen, T. Onishi, and H. Nozoye, *Appl. Phys. Lett.*, **59**, 1793 (1991).
14. M. Hara, K. Domen, T. Onishi, and H. Nozoye, *J. Phys. Chem.*, **95**, 6 (1991).
15. M. Hara, K. Domen, T. Onishi, H. Nozoye, C. Nishihara, Y. Kaise, and H. Shindo, *Surf. Sci.*, **242**, 459 (1991).
16. A. Winkler, C. Resch, and K. D. Rendulic, *J. Chem. Phys.*, **95**, 7682 (1991).
17. E. L. Crane and R. G. Nuzzo, *J. Phys. Chem. B*, **105**, 3052 (2001).
18. E. P. Go, K. Thuermer, and J. E. Reutt-Robey, *Surf. Sci.*, **437**, 377 (1999).
19. M. Pourbaix, *Atlas of Electrochemical Equilibria in Aqueous Solutions*, p. 638, Pergamon, New York (1966).
20. B. J. Wiersma, Y. Tak, and K. R. Hebert, *J. Electrochem. Soc.*, **138**, 371 (1991).
21. A. J. Bard and L. R. Faulkner, *Electrochemical Methods: Fundamentals and Applications*, Wiley, New York (2001).
22. H. C. Lee, F. Xu, C. S. Jeffcoate, and H. S. Isaacs, *Electrochem. Solid-State Lett.*, **4**, B31 (2001).
23. C. J. Boxley, J. J. Watkins, and H. S. White, *Electrochem. Solid-State Lett.*, **6**, B38 (2003).
24. C. J. Boxley and H. S. White, *J. Electrochem. Soc.*, **151**, B265 (2004).
25. S. Lee and H. S. White, *J. Electrochem. Soc.*, **151**, B479 (2004).
26. T. Hurlen and A. T. Haug, *Electrochim. Acta*, **29**, 1133 (1984).
27. W. Wilhelmsen and T. Hurlen, *Electrochim. Acta*, **32**, 95 (1987).

28. J. Newman and K. E. Thomas-Alyea, *Electrochemical Systems*, Wiley, Hoboken, NJ (2004).
29. R. S. Alwitt, in *Oxides Oxide Films*, J. W. Diggle and A. K. Vijh, Editors, p. 169, Marcel Dekker, New York (1976).
30. A. C. Harkness and L. Young, *Can. J. Chem.*, **44**, 2409 (1966).
31. T. Valand and K. E. Heusler, *J. Electroanal. Chem.*, **149**, 71 (1983).
32. K. R. Hebert, H. Q. Wu, T. Gessmann, and K. Lynn, *J. Electrochem. Soc.*, **148**, B92 (2001).
33. H. K. Birnbaum, C. Buckley, F. Zeides, E. Sirois, P. Rozenak, S. Spooner, and J. S. Lin, *J. Alloys Compd.*, **253–254**, 260 (1997).